

Effects of Fence on the Spanwise Aerodynamic Characteristics of an Aircraft Wing Profile with Various Taper Ratios

T. A. Sundaravadivel^{1†}, E. Karthik Vel², and S. Nadaraja Pillai²

¹ Faculty of Mechanical Engineering, R.M.D. Engineering College, Chennai, Tamil Nadu-601206, India

² School of Mechanical Engineering, SASTRA Deemed to be University, Thanjavur, Tamil Nadu-613401, India

†Corresponding Author Email: tas.snh@rmd.ac.in

ABSTRACT

This paper investigates the effects of the chordwise fence on the spanwise change in aerodynamic characteristics of an aircraft wing with a different taper ratio for varying angles of attack. The investigation was carried out for the tapered wing with different taper ratios of 0.41, 0.6, and 0.75. The wing is tested in a subsonic, low turbulence wind tunnel at the free stream Reynolds number of 2.3×10^5 for various angles of attack ranging from $\alpha = 0^\circ$ to 45° . The baseline wing model is attached to a fence of different diameters of 1.5 and 2.5 mm at a plane equal to the root and tip chord. There are pressure ports spread across the span of the wing, and the corresponding surface pressure is measured using the MPS 4264 miniature pressure scanner. The surface pressure measured is analyzed further for the variation of the aerodynamic characteristics of the wing. The presence of a fence on the tapered wing forms an efficient flow control device that delays the flow separation, thereby delaying stall angles and preventing the steep transition of the favorable pressure gradient to the adverse pressure gradient at the stall. The presence of a fence on the wing surface has considerably increased the lift coefficient, and the stall is significantly delayed for a least taper ratio wing. The fence has suppressed the interaction of the leading-edge vortices with the tip vortices; thereby, the spanwise flow from the root chord to the tip chord is controlled.

Article History

Received December 17, 2023

Revised February 12, 2024

Accepted February 26, 2024

Available online May 29, 2024

Keywords:

Fence mean chord ratio

Lift coefficient

Pressure coefficient

Wind tunnel testing

Spanwise flow

1. INTRODUCTION

The design of a wing, particularly its shape and geometry, plays a vital role in determining its aerodynamic characteristics. Tapered wings, characterized by a gradual reduction in wing width from root to tip, have been widely adopted in aerospace engineering due to their potential benefits in terms of favourable lift distribution, reduced drag, and improved structural integrity. This research paper aims to comprehensively investigate the aerodynamic characteristics of tapered wings with various taper ratios, focusing particularly on understanding the behaviour of spanwise flow patterns. By analyzing and evaluating the complex flow interactions along the wingspan, valuable insights can be gained to optimize the design of tapered wings and enhance overall aircraft performance.

Several studies have investigated the effects of the taper ratio on the lift distribution, drag characteristics, and spanwise flow patterns. A study by Güzelbey et al. (2019) revealed that there is an optimum taper ratio for a wing

that has a minimum induced drag coefficient and maximum Oswald efficiency factor. However, decreasing the taper ratio too much can cause wingtip stalls due to higher local lift coefficients at the tip region of the wing; conversely, a higher taper ratio increases the size of the wingtip vortices. Therefore, finding the right balance in the taper ratio is important for optimizing lift and drag in a wing design. In the application of micro air vehicles (MAVs), flexible wings are predominantly utilised, and the study by Yang et al. (2012) involved flapping wings with a high stiffness leading edge and more flexible chord ribs to limit spanwise deformation in small range and maintain chordwise deformation in a suitable range. This can cause a stronger backward flow to increase the thrust, which can improve the aerodynamic performance of FMAVs.

A study by Krishnan et al. (2020) with a Ruppell griffon vulture (RGV) - type winglet demonstrated a 15% to 30% reduction in the drag coefficient and a 5% to 25% increase in the lift coefficient when using an RGV winglet. The vortical structure sheds in a non-uniform manner across the span of the wing and the spanwise distribution

NOMENCLATURE			
α	angles of attack (°)	<i>MAV</i>	Micro Air Vehicle
C_L	coefficient of lift	X/c	non-dimensional chord
C_P	coefficient of pressure	<i>RGV</i>	Ruppel's Griffon Vulture
C_D	coefficient of drag	<i>VG</i>	Vortex Generator
C	chord length in (m)	ϕ	flow coefficient
<i>FMCR</i>	Fence Mean Chord Ratio		

of force coefficients is related to the three-dimensional wake dynamics and tip effects. Thus, at higher angles of attack, the influence of the unsteady vortical structure on the flow separation phenomenon was explained by [Zhang et al. \(2020\)](#). The uncontrollably shed vortices have a random nature except for the rotating wing, where the spanwise random motion vortices are very short; thus, these shed vortices are collectively balanced by vorticity annihilation and Coriolis tilting, as stated by [Eldredge and Jones \(2019\)](#). Many numerical models have been developed to understand the evolution of the vortical structure interaction between the leading-edge vortex and the tip-induced vortices. The spanwise flow on the swept-back wings, which promotes the separation of flow from the wing tips, has been studied using various active flow control techniques, one of which employs a fluidic oscillator, where the spanwise flow is redirected in the streamwise direction, reducing the separation. Thereby the associated drag coefficient decreases ([Wang et al., 2019](#)). Research performed by [Hao et al. \(2023\)](#) on the different height distributions of VGs (Vortex Generators) across the span induces a great deal of increase in aerodynamic characteristics such as lift, stall delay, and flow separation. Several investigations have been performed to study the transition of flow characteristics in the presence of vortex generators in aircraft wings ([Arunvinthan et al., 2021](#)), wind turbines ([Wang et al., 2021](#)), and dynamic stalling ([De Tavernier et al., 2021](#)). The high-energy vortices generated by the vortex generator on the airfoil surface of the wind turbine investigated by [Wu et al. \(2022\)](#) energized the flow, thereby inducing an increase in the momentum of the flow in the boundary layer. [Richard et al. \(2017\)](#) visualized the coherent flow structure in the presence of leading-edge slats, thereby identifying the nature of the structure and the corresponding interaction of the vortex structure between the slat and airfoil surface causing strong acoustic waves. Research performed by [Joseph et al. \(2022\)](#) revealed that the presence of leading edge serration on a wing structure and wind turbine blades leads to an increase in the post-stall aerodynamic improvement and overall efficiency of approximately 2 to 11% and a reduction in the structural load caused by external winds of 7 to 17%, the passive device has reduced the vibration on the body induced due to the vortex shed. Similarly, a study implementing helical semicircular spiral protrusion has reduced vibration caused by the vortex shed from the surface ([Koca & Ozturk, 2022](#)). A study by [Rezaeiha et al. \(2019\)](#) proved that a leading surface suction slot improved the aerodynamic efficiency and flow separation delay, thereby strongly influencing the dynamic stall phenomenon. Similarly, multiple suction jets ([Elsayed et al., 2023](#)) were employed on the wing section, imparting variation in the aerodynamic characteristics with an increase in C_L of 55.7% and

considerable stall delay. [Raj Mohamed et al. \(2021\)](#) studied different types of nose structures from cetacean species that were inspired and inducted instead of the leading edge of the NACA 6 series airfoils and the authors improved the aerodynamic results in the post-stall regions. The presence of protrusions at various locations on the suction surface was investigated by [Bodavula et al. \(2019\)](#), and an increase in the aerodynamic lift of approximately 59% was observed. A recent study on a surface-modified airfoil has shown that the gapped model has better aerodynamic performance than the stepped model in comparison to the standard model ([Öztürk et al., 2023](#)). A research study by placing the stall fence on the wells turbine has shown a 16.6% improvement in operating range at the cost of peak torque developed by the turbine and the peak-to-average power ratio in the stall-free range is reduced by 16.7% when stall fences are used. Figure 1 represents the formation of vortices for the reference turbine and the fenced turbine explaining the delay in the formation of the starting vortex for the fenced turbine at three different flow coefficients ([Das & Samad, 2020](#)).

The wing fence has been widely used for non-rotating applications: especially for aircraft with swept wings and was found to be a good entrant for aerodynamic performance improvement. Wind tunnel visualization and theoretical studies by [Rudenko and Ryzhkova \(1968\)](#) and [Rossow \(1992\)](#) suggested that the use of a wing fence for swept-wing aircraft produces a vortex outboard of the fence, that rotates in the opposite direction to the wing tip vortex. [Williams et al. \(2010\)](#) used boundary layer fences in T-38 Talon aircraft and performed simulation and flight tests to optimize the dimensions and spanwise locations of the fence. [Armstrong et al. \(2012\)](#) employed boundary layer fence to vertical axis wind turbine blades with canted blades and observed power increase and reduction in the blade speed ratio which was a result of the reduction in spanwise flow on the swept blades and found that the blades locally behave similar to straight blades. [Sundaravadivel et al. \(2013a, b\)](#) studied the performance of a fence attached to a rotating wind turbine blade set and found a good improvement in power performance & and also added that the induced drag has been decreased due to alteration in downwash distribution.

Figure 2 illustrates how the fences keep the flow linked to the suction surface from leading to trailing edges at varying flow coefficients. For the reference turbine, the flow is coupled to the suction surface close to the leading edge at $\phi = 0.225$. As shown in Fig. 2, the separation begins to happen close to the trailing edge. In the vicinity of the reference turbine's tip area, tip leakage vortices are seen. The tip leakage vortices in the fenced turbine are shifted at 80% chord length from the tip region towards

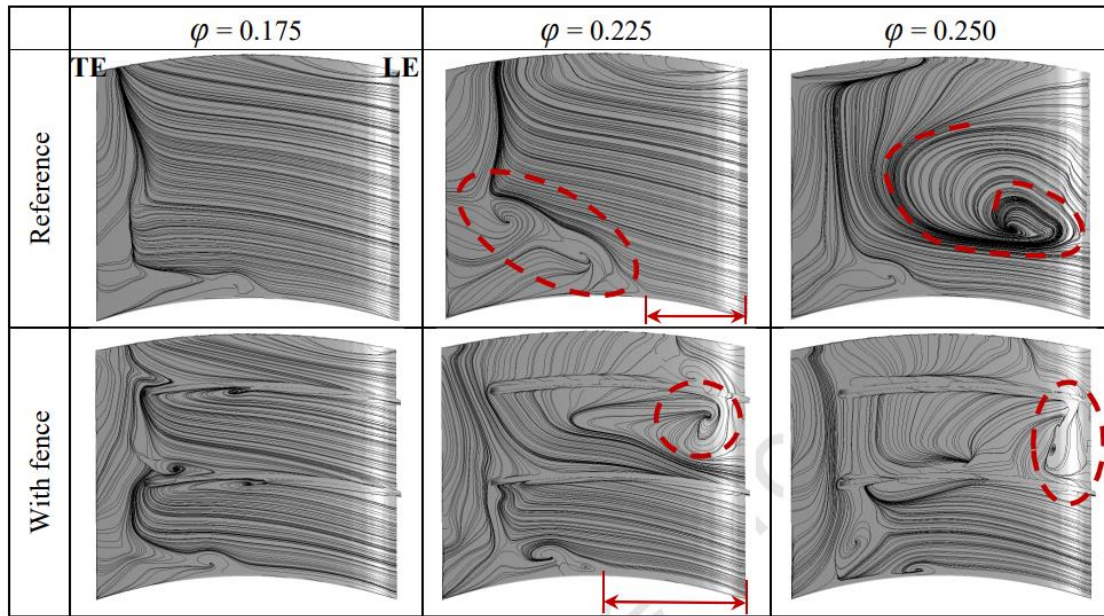


Fig. 1 Streamline for the turbine blade at different flow coefficients (Das & Samad, 2020)

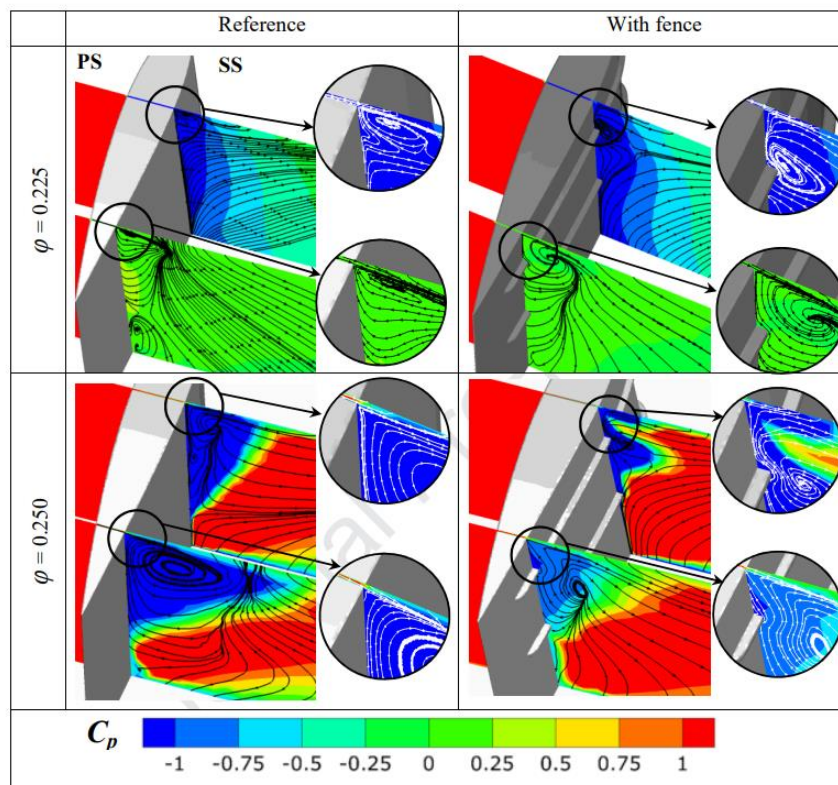


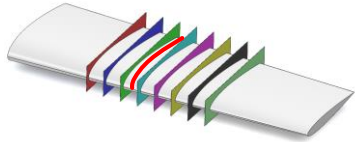
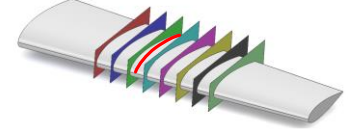
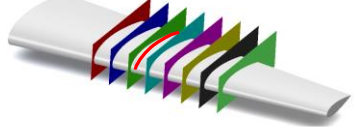

Fig. 2 Streamline for the turbine blade at different flow coefficient

the fence. For the reference turbine, the vortex generation and flow separation are more noticeable at $\phi = 0.250$.

This research study introduces a chordwise fence on the suction and pressure sides of wings with different taper ratios. The fence was introduced at the plane of the tapered wing, the investigation was carried out for different diameters, and the surface pressure across the wing span was recorded. Understanding of the presence of

a chordwise fence in the transition of flow across the span for wings of various tapered ratios is still lacking, as proper investigations concerning the broad spectrum of prior research have been carried out. This finding encouraged us to use boundary layer fences based on the abovementioned literature survey. This research investigation helps us understand the effects of spanwise flow on different fence diameters and how the corresponding aerodynamic characteristics are influenced

Table 1 Model specification of various taper wings used for the investigation and with different fences attached and the corresponding Fence Mean Chord Ratio used for the investigation

Wing Model	Wing Specification (m)		Wing Model	Diameter of the fence, d (mm)	FMCR
	Root Chord	0.1	Model 1	1.5	0.017
	Tip Chord	0.075		2.5	0.029
	Taper Ratio	0.75			
	Root Chord	0.1	Model 2	1.5	0.019
	Tip Chord	0.06		2.5	0.031
	Taper Ratio	0.6			
 <p style="text-align: center;">Fence</p> 	Root Chord	0.1	Model 3	1.5	0.021
	Tip Chord	0.041		2.5	0.035
	Taper Ratio	0.41			

by various taper ratios of wings and this ultimately provides scientific data to the research community.

2. EXPERIMENTAL SETUP

A series of wind tunnel investigations were performed on a wing with three different taper ratios at the wind tunnel facility with a free stream velocity of 30 m/s corresponding to a Reynolds number of 2.3×10^5 is considered to be the transitional Reynolds number ($10^5 - 3 \times 10^5$). The study under transitional flows helps us understand both laminar and turbulent flow phenomena and the aerodynamic characteristics obtained for the transitional regime will help us design wings for improved aerodynamic efficiency. The NACA 6-digit series airfoil NACA 63(4)-021 is used as the basic airfoil profile for the construction of the wing.

The details of the model are given in Table 1, where eight different planes intersect the wing's surface at various locations across the span of the wing. The model specifies the planes where the pressure data are recorded across the span of the wing to understand the variation in aerodynamic characteristics. For each wing, a fence with two different diameters has been employed and experimental investigation have been performed. Thus, a parameter called the Fence Mean Chord Ratio (FMCR) has been used to correlate the wing with different taper ratios, and the addition of a fence with two different diameters. The different cases considered for the investigation are tabulated in Table 1.

The fence is placed in the gap between the third and fourth planes along the span, which accounts for 44% of the span length from the root chord. The Fence Mean Chord Ratio (FMCR) is defined as the ratio of the diameter of the fence introducing the suction surface of the wing to the mean aerodynamic chord length of the wing, where C_{mean} is the mean of both the root and tip chord of the wing.

Figure 3 shows a schematic of the wind tunnel setup used for the investigation, where the wing model is mounted at the test section. The model has approximately 6 pressure taps in the chordwise planes and there are 8 such planes at various locations across the span of the wing. A total of 48 pressure ports are present on the suction surface of the wing, similar to the pressure side of the wing. To sense the surface pressure and record the time-varying data, an ethernet-based multichannel pressure scanner, which is an independent processor used to transfer the time series data by establishing a network between the sensor and the computer system. The pressure taps are connected to the scanner using polyurethane tubes.

2.1 PRESSURE MEASUREMENT:

The surface pressure spread across the wings was measured by using MPS 4264 an ethernet-based simultaneous pressure scanner. The sampling frequency of about 700 Hz which accommodates a total pressure sample of 10000 data from each of the pressure ports suspended on the wing surface for a time of 14.3 seconds is used for the investigation. The raw pressure data measured from the surface of the wing with and without a fence is presented in Fig. 4. Further, the aerodynamic coefficients and the surface pressure coefficients are measured based on the approach followed by [Arunvinthan et al. \(2020\)](#), [Arunvinthan and Nadaraja Pillai \(2019\)](#); [Sundaresan et al. \(2021\)](#).

3. RESULTS AND DISCUSSION

3.1 Variation of Aerodynamic Coefficient for the wing with and without Fence

The variation in the coefficient of lift corresponding to the angle of attack (α) for Model 3 for varying FMCRs is shown in Fig. 5e. The coefficient of lift is calculated based on the average pressure coefficient taken across different planes of the pressure ports in the chordwise direction. The

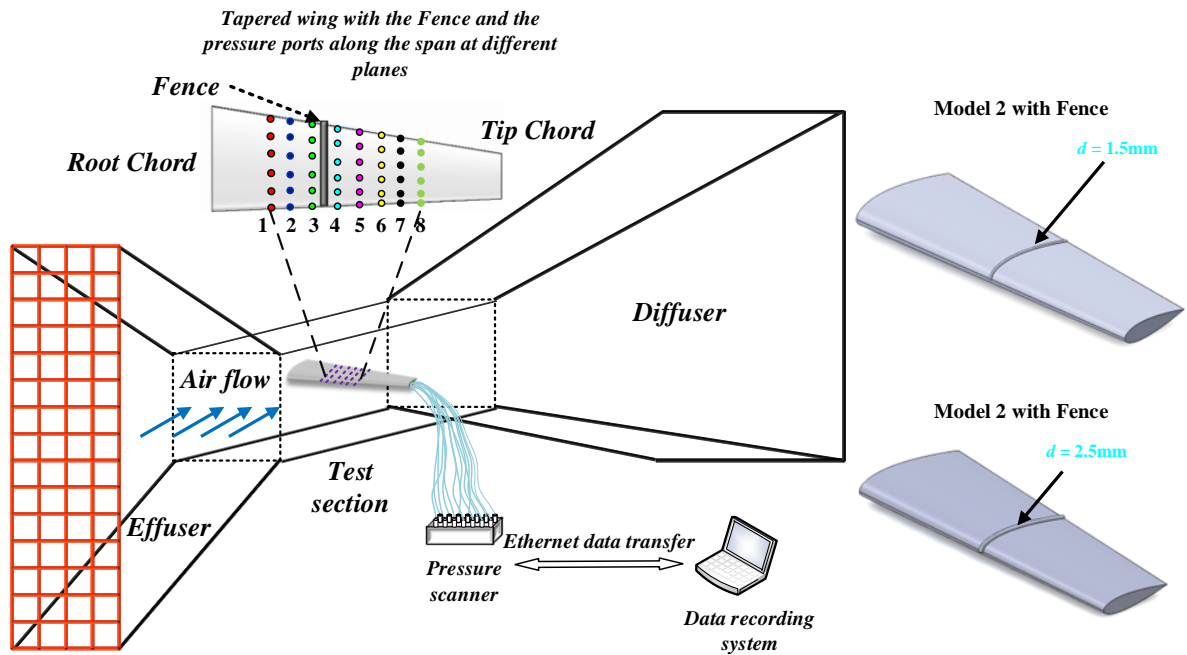


Fig. 3 Schematic of the experimental setup for the investigation

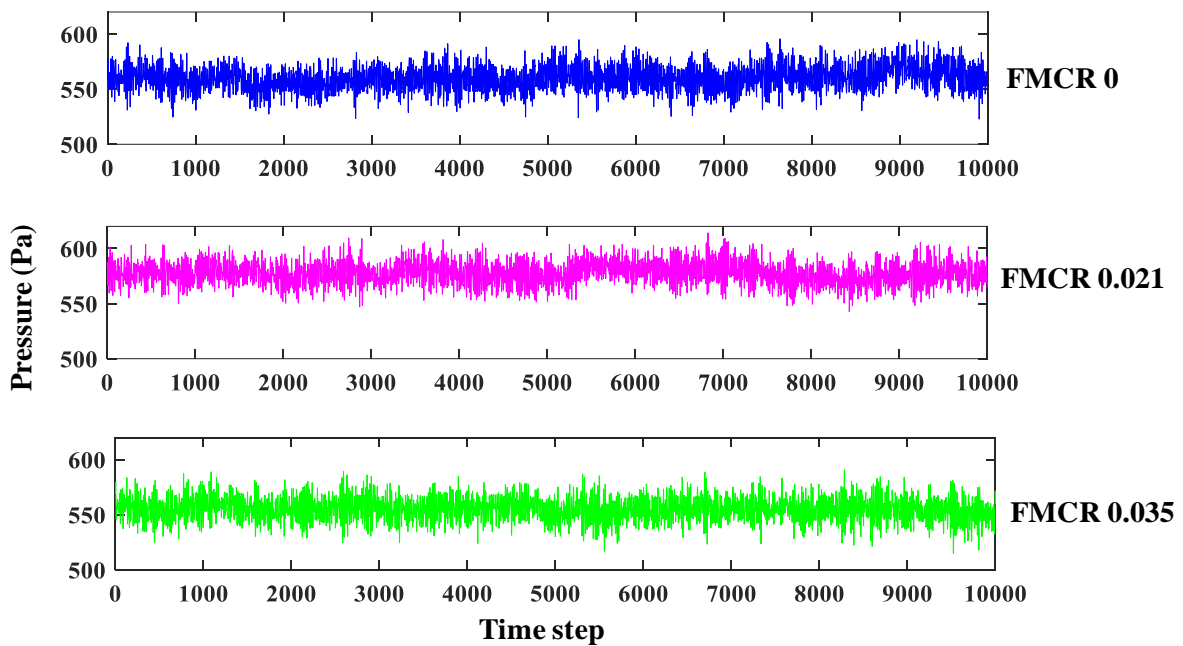
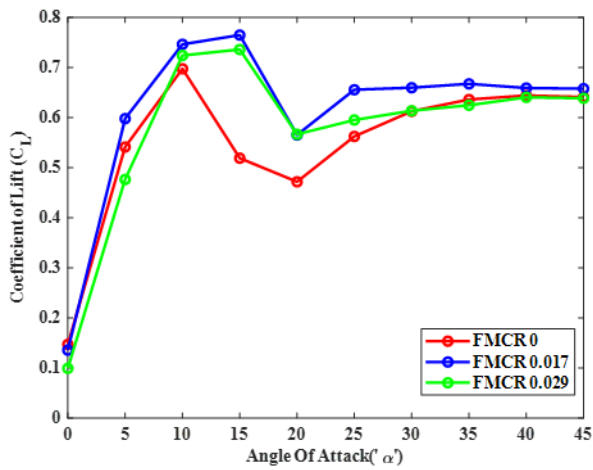


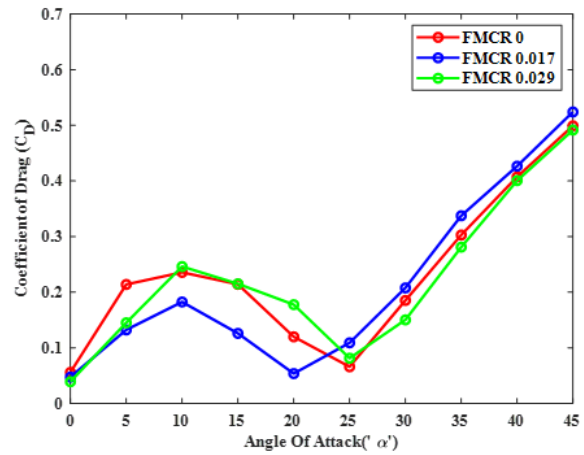
Fig. 4 Raw surface pressure data from the suction surface of the wing configuration with and without the fence. The pressure data from the port at plane 4 and x/c of 0.4 at 5° angle of attack.

aerodynamic coefficients are calculated based on the average pressure. Model 3 with $FMCR = 0$ shows an increase in the lift and the maximum lift is achieved at an angle of attack of 10° . Furthermore, a stall is observed, followed by a recovery in pressure. The addition of a fence considerably increased the lift coefficient at all angles of attack, particularly at $FMCR = 0.035$, for which the stall angle was increased to 15° . There seems to be an increase in the lift slope in the pre-stall region for the wing with the fence attached. Furthermore, a fence with a diameter of 2.5 mm and an $FMCR$ of 0.035 exhibited an increase in the stall angle of 5° . Similarly, Fig. 5c reveals the variation

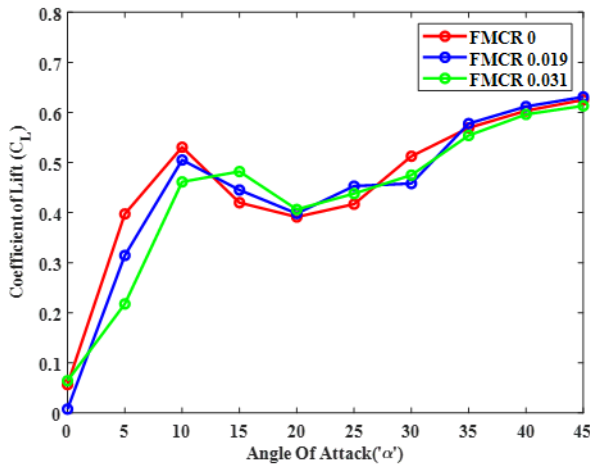
in the coefficient of lift for Model 2 for varying fence diameters. Here, the addition of a fence has shown an increase in lift, yet the stall characteristics seem to be slightly smoother than those of Model 3. The maximum lift is observed for Model 2 in the poststall region. Model 2 encounters a different phenomenon with a decrease in the lift for almost all angles of attack with the attachment of the fence in comparison, the wing with $FMCR = 0.031$ shows an additional delay in the stall angle of 5° . Model 1 manifests a comparatively better increase in aerodynamic characteristics than Model 2 and Model 3.



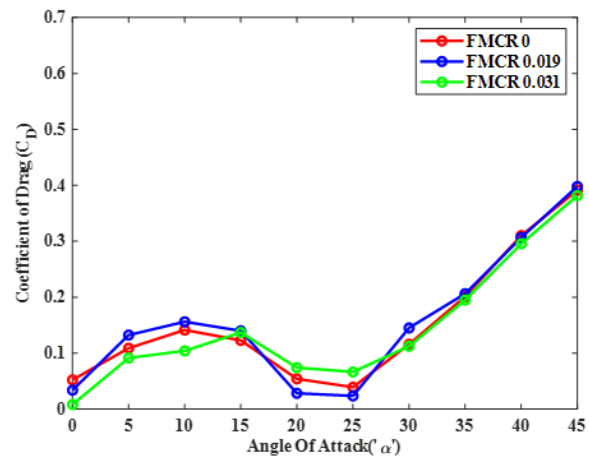
5a. Model 1



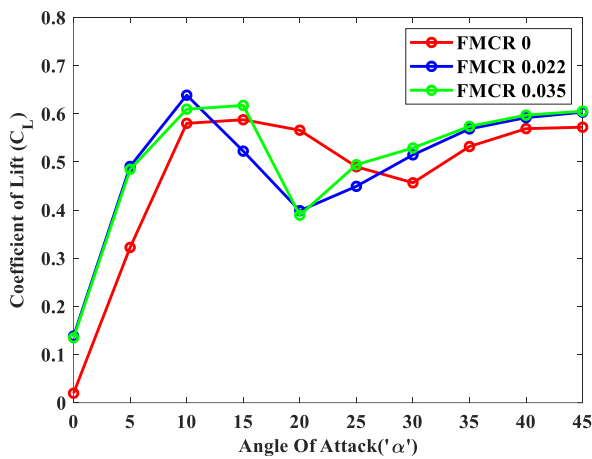
5b. Model 1



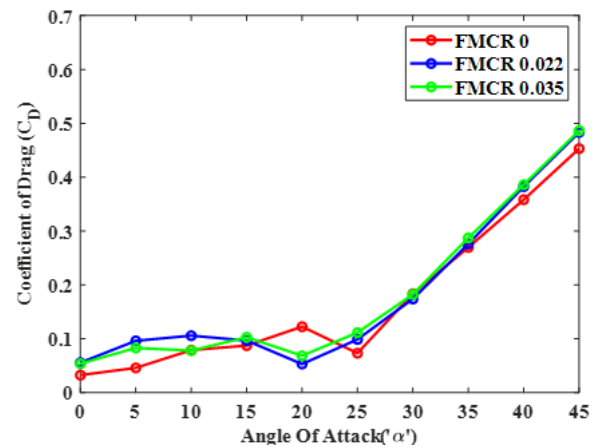
5c. Model 2



5d. Model 2



5e. Model 3



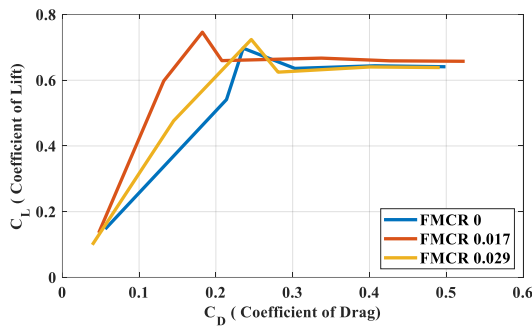
5f. Model 3

Fig. 5 Variation of coefficient of lift and coefficient of drag for models 1, 2 &3

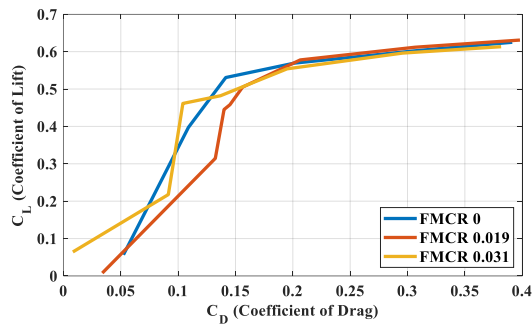
Figure 5a shows the variation in the coefficient of lift for Model 1. The coefficient of lift increases drastically for the wing with a minimum taper; thus, the presence of a fence increases the stall angle by $\alpha = 5^\circ$. The above graphs confirm that the presence of fences alters the boundary layer on the surface of the wing, thereby increasing the lift slope when compared with that of the wing without a fence. Alternatively, in the post-stall region, the shreds of evidence of turbulence flow generation because of the

presence of a fence potentially improved the lift irrespective of the tapering ratio of the wing.

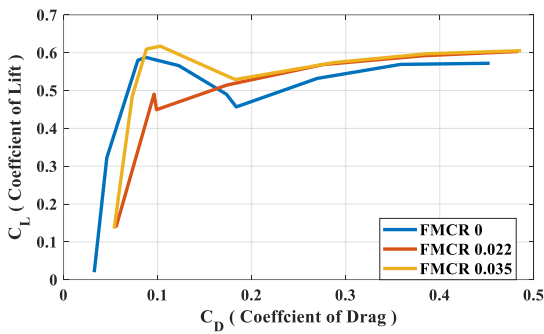
The drag coefficients of wing model 3 with various fences are shown in Fig. 5f. The drag coefficient of the wing model with the fence reveals an increase in drag in the pre-stall region; conversely, in the stall region, there is a drastic decrease in drag followed by similar drag behaviour in the poststall region when compared with that of Model 3 without the presence of a fence. As the taper



a) Model 1



b) Model 2



c) Model 3

Fig 6 Plot between Coefficient of lift (C_L) and Coefficient of drag (C_D) for various wing models with and without fence

ratio of the wing increases for Model 2, the drag coefficient shows a different phenomenon until the stall.

The model without the presence of any fence shows a region of a slight bump in the pre-stall region followed by a linear increase in the drag coefficient. Figure 5d shows that the magnitude of drag is less than the corresponding drag component of Model 3 in the poststall region.

Model 2 with $FMCRC = 0.031$ shows a considerable decrease in the drag coefficient when compared with that of Model 2 with $FMCRC = 0$. Model 1, which has the least taper ratio, has a different drag characteristic, where the wing with $FMCRC = 0.017$ has the least drag in the pre-stall region; conversely, in the poststall region, the drag increases and this is shown in Fig. 5b.

In the current investigation, Fig. 6 shows the plot of C_D to C_L for the three different tapered models with two different fences. An increase in the C_{Lmax} has been found for Model 1, which has having lower taper ratio and more surface area when compared to the same wing without the fence. A similar situation is observed for Model 3 where the C_{Lmax} is found to be at a lesser C_D when compared to Model 1, which signifies the decrease in the surface area Model 3 has resulted in the improvement in the lift component at a lower induced drag. The shift in the plateau signifies the increase in the drag however it decreases with the decrease in the taper ratio. Figure 6a shows a plateau which signifies the maximum lift followed by the decrease in the lift indicating the stall region, however, the gradient of the C_L to the C_D is more for Model 1 with the presence of a fence indicating the increase in the aerodynamic efficiency. For Model 3, the gradient for the modified model is similar to the base model and the negative zero lift angle of attack observed for the modified model is seen in the Fig. 6c with the increase in the C_{Lmax} for Model 3 with $FMCRC = 0.035$. Deep Stall characteristics are observed with a plateau which is seen for Model 1 and Model 3, however, there is no significant plateau observed for Model 2, which signifies the occurrence of the smooth stall phenomenon.

3.2 Variation of Surface Pressure Coefficient for the Wing with and without Fence

Figure 7 shows the three-dimensional plot of the coefficient of pressure across various planes along the

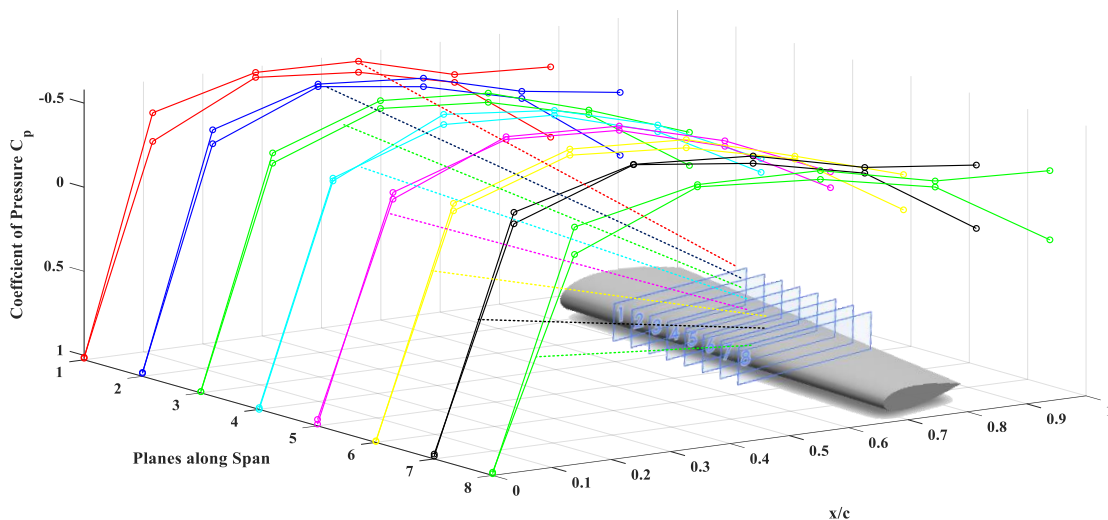


Fig. 7 Schematic representation of coefficient of pressure at various planes from root to tip of the wing

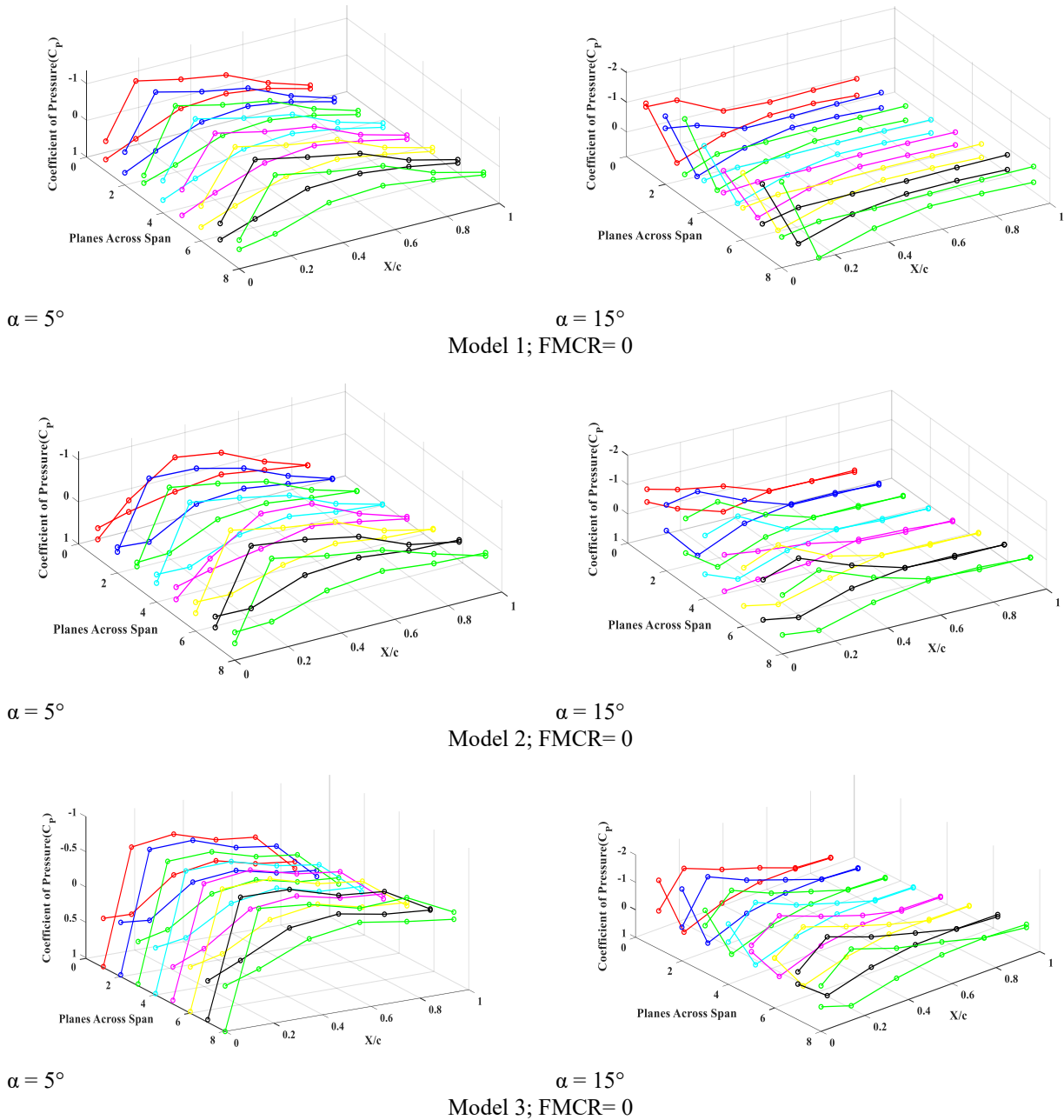


Fig. 8 The C_p variation of Model 1, 2 and 3 with FMCR = 0 across the span for 5° and 15° angles of attack

span of the wing. Planes 1 to 8 represent each plane across the span from the root to the tip of the wing and are correspondingly represented with a different colour. The pressure across the span of the wing at each angle of attack is represented in a 3D plot, which helps to understand the variation in depth to determine the effects of spanwise flow. Correlating the aerodynamic lift and drag characteristics observed for Model 1 with FMCR = 0, the pressure variations in the corresponding models across the span at 8 different locations for angles of attack of 5° and 15° for the three different models are shown in Fig. 8. When the angle of attack increases, there is an increase in the negative pressure on the suction surface and vice versa on the pressure side of the wing until $\alpha=10^\circ$, associated with the maximum lift coefficient in Fig. 5a, where the maximum difference in pressure is observed between the suction and pressure sides of the wing.

At an angle of attack of $\alpha=15^\circ$, there is a decrease in the pressure on the upper surface of the wing compared with that at $\alpha=10^\circ$, however, there is low pressure at the first two planes from the root of the wing further along the span and there is comparatively higher pressure observed as shown in Fig. 8. This signifies the spanwise flow generated from the tip to the root of the wing. Furthermore, an increase in the angle of attack resulted in a constant pressure line on the upper surface, indicating detachment of the flow from the surface of the wing. On the pressure side of the wing, with increasing angle of attack, the pressure gradient seems to increase, and proper recovery is observed. Especially near the trailing edge, the pressure on the lower surface is greater than that on the upper surface; therefore, evident flow separation occurs; however, the pressure difference is compensated for by the

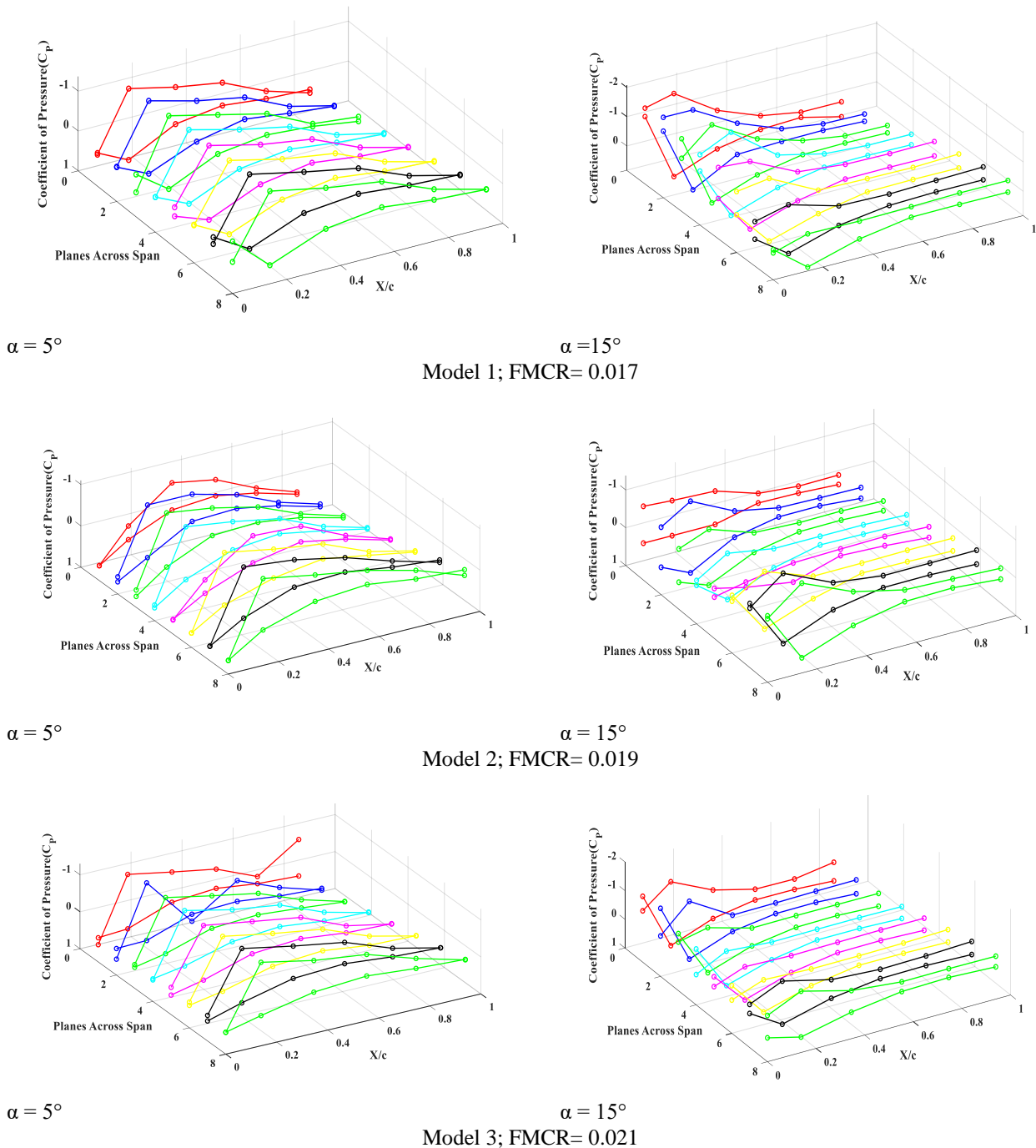


Fig. 9 The C_p variation of Model 1, 2 and 3 with different FMCR (15 mm Fence diameter) across the span for $\alpha = 5^\circ$ and $\alpha = 15^\circ$ angles of attack

increase in lower surface pressure, which accounts for the increase in lift in the poststall region.

The presence of the fence on the wing induces intermittent low pressure on the suction surface, causing momentum near the location of the fence at immediate stall angles, thereby suppressing spanwise flow interactions due to tip vortex inflow. The coefficient of lift is found to be less than that of Model 1, and this is evident from the surface pressure for Base Model 2 with an FMCR of 0. When there is an addition of a fence with an FMCR of 0.031, we can observe an increase in the stall angle from the previously ranged $\alpha = 10^\circ$ to $\alpha = 15^\circ$, and the stall seems to be relatively smooth. At the least taper ratio, when we

add the fence to the wing, we can observe evidence for an increase in the lift coefficient with an FMCR of 0.021 and a delay in a stall with a considerable increase in negative suction pressure at $\alpha = 15^\circ$, as shown in Fig. 9. The surface pressure at plane 2 shows a steep pressure gradient and recovery, which helps us understand the increase in momentum of the flow caused by the presence of the fence. Figure 10 shows the pressure distributions of all the models with a 2.5 mm diameter fence. The increase in the coefficient of Lift at $\alpha = 15^\circ$ is evident from the increase in the pressure difference for Model 1 and Model 3; similarly, the decrease in the pressure difference in Model 2 correlates with the aerodynamic characteristics depicted in Fig. 5.

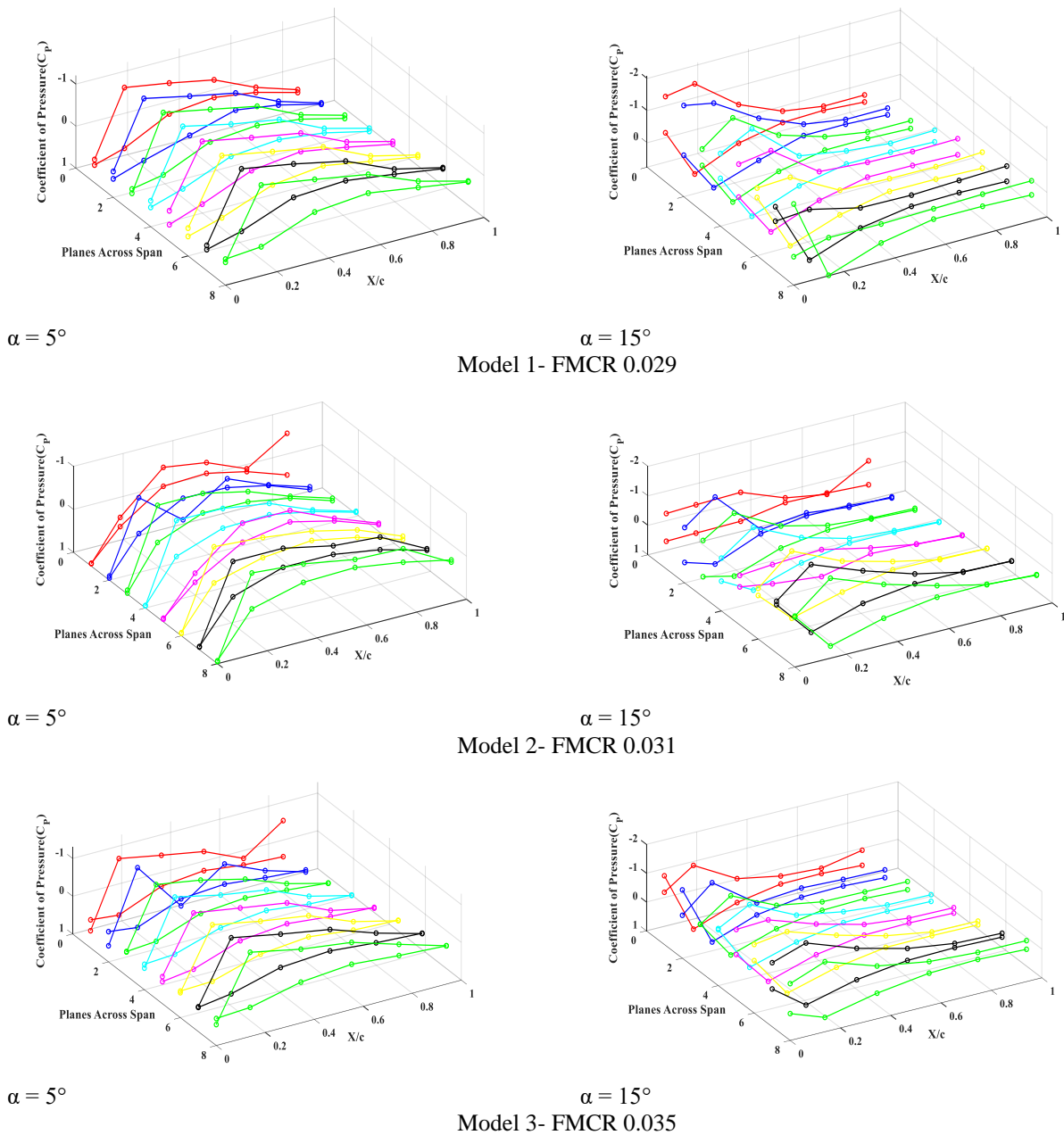
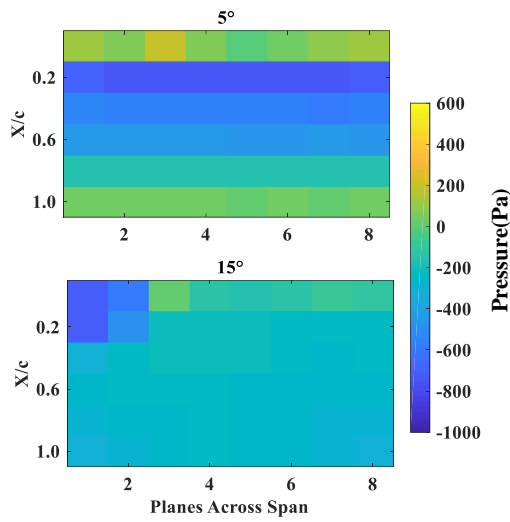


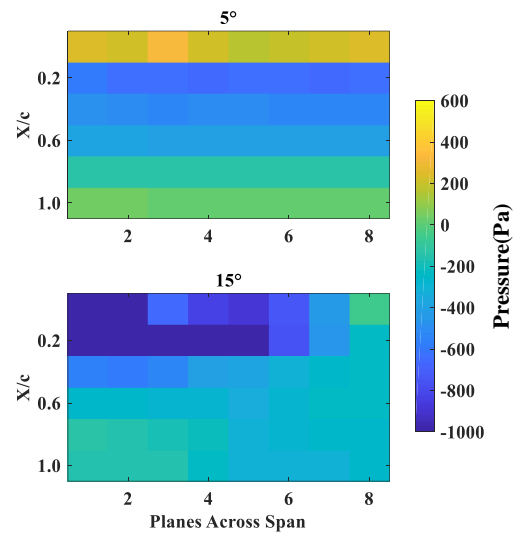
Fig. 10 The C_p variation of Model 1, 2 and 3 with different FMCR across the span for 5° and 15° angles of attack

Figure 11 shows a colour map of the surface pressure measured from Model 1 and Model 3 with and without a fence to determine the detailed effects of the presence of the fence. The colour map clearly shows the increase in suction surface pressure for $\alpha = 15^\circ$ for Model 1 with FMCR = 0 and 0.029. An increase in momentum with the presence of the Fence with FMCR = 0.029 is observed at the stall and poststall angles of attack. Figure 11a shows the inflow from the tip chord direction to the root chord direction at $\alpha = 15^\circ$, and the flow in the trailing surface is detached near the tip chord of the wing, whereas it is associated with a favourable pressure gradient for an attached flow at the root chord. When we increase the diameter of the fence, a high-pressure area forms near the fence on the suction surface that considerably reduces the spanwise flow from the tip chord to the root chord, as

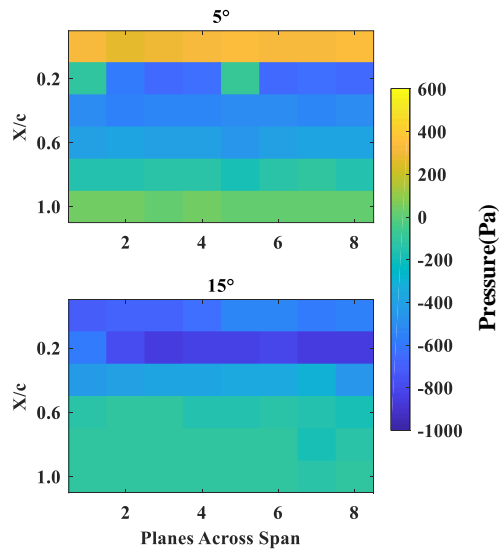
shown in Fig. 11b. At $\alpha = 15^\circ$, the model with FMCR = 0 has a comparatively greater pressure on the suction surface from the root to the tip chord, which is evident from Fig. 11a. Similarly, at FMCR = 0.029, the higher pressure earlier on the span toward the root chord is suddenly changed to a considerable area of the low-pressure region toward the root chord region, thereby decreasing the intensity of the high-pressure zones. This finding provides evidence that spanwise flow is suppressed by the presence of a 2.5 mm diameter fence, decreasing the pressure difference, which causes the momentum of flow from the tip to the root of the wing. When the taper ratio of the wing is increased, we can see that there is a slight increase in the lift coefficient with the addition of the fence, this is also evident from the colour contours on the suction surface, as shown in Fig. 11e and Fig. 11f, at $\alpha = 15^\circ$.



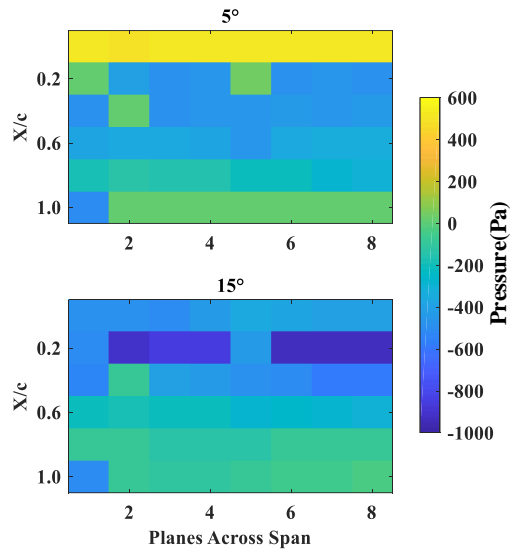
11a. FMCR = 0



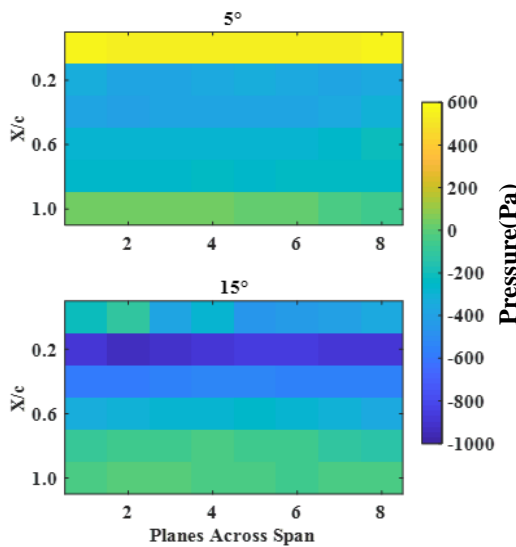
11b. FMCR = 0.029
Model 1



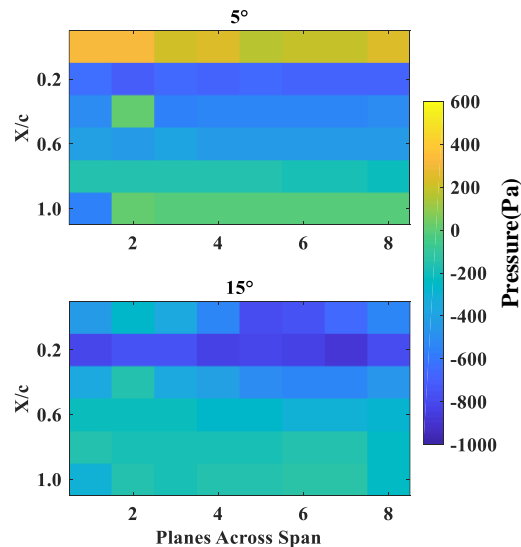
11c. FMCR = 0



11d. FMCR = 0.031
Model 2



11e. FMCR = 0



11f. FMCR = 0.035
Model 3

Fig. 11 Colour map of the wing model with and without the Fence

Figures 11c and 11d show the suction surface pressure for Model 2 at the angle of attack of $\alpha = 5^\circ$ and 15° , at low angle there is a slight increase in the pressure near the root chord and the presence of the lower pressure in the tip chord region. When the angle is further increased to $\alpha=15^\circ$ for model 2, the presence of the fence has drastically increased the pressure in the root chord region when compared to the tip chord region. However, there is a further increase in the negative pressure on the suction surface increasing the lift coefficient. For the wing model with maximum taper, the ratio shows a significant increase in the negative pressure in the root region, however, there is a small positive pressure region in the tip section. This shows the infusion of flow from tip to chord as seen in Model 1 without a fence is reduced to a greater extent. When the taper ratio is decreased further the negative pressure spreads all across the suction surface at a high angle of attack, with a considerable high pressure region formed near the fence thereby following the above flow phenomena. For the least taper ratio model there is widespread negative suction pressure in the tip chord region however the positive pressure near the fence is further increased preventing spanwise flow and showcasing an efficient aerodynamic improvement with sustained peak negative pressure, delaying stall and separation of flow from the suction surface.

4. CONCLUSION

The present experimental investigation was performed for wing configurations with various taper ratios and the variation in aerodynamic characteristics is understood with the presence of a fence on the wing at a particular Reynolds number of 2.3×10^5 . In addition to aerodynamics, spanwise flow characteristics have been thoroughly studied. The following conclusions were drawn from the investigation:

1. Naturally, the coefficient of lift is increased by 16.5% for the least tapered wing when compared with the most tapered wing.
2. The addition of a fence on the wing surface improved the aerodynamic performance of the wing model with the highest taper ratio (Model 3). The coefficient of lift is increased by 5% for FMCR = 0.021 and by 7.2% for FMCR = 0.035.
3. Similarly, the fence on the wing model with the least taper ratio (Model 1) has significant lift characteristics. The lift coefficient is increased by 13.2% for FMCR = 0.017 and by 6% for FMCR = 0.029.
4. A significant stall delay was observed when a fence was added to the wing model with a least tapering ratio (Model 1) of approximately 5° .
5. The spanwise flow from the tip to the root of the wing was identified for the baseline wing with the maximum taper ratio (Model 3), which was suppressed by the presence of fences of different diameters, as indicated by the coefficient of pressure and the cooler map. The momentum induced by the presence of a fence successfully reduced the

interaction of the tip vortices with the leading-edge vortices that formed on the wing.

Furthermore, an extensive study of the variation in spanwise flow with fences at multiple locations along the span will provide in-depth insight into the spanwise flow characteristics.

ACKNOWLEDGEMENTS

This research work was supported by the Science Engineering Research Board (SERB), Department of Science & Technology (DST), Government of India, File No: CRG/2021/005720.

CONFLICT OF INTEREST

The authors declare that they do not have any competing interests.

AUTHORS CONTRIBUTION

T. A. Sundaravadivel conceived & designed the experimental methodology and performed the analysis. **E. Karthik Vel** and **S. Nadarajapillai** collected the data and wrote the paper. All the authors equally contributed to the result analysis and deriving inferences.

REFERENCES

- Armstrong, S., Fiedler, A., & Tullis, S. (2012). Flow separation on a high Reynolds number, high solidity vertical axis wind turbine with straight and canted blades and canted blades with fences. *Renewable Energy*, *41*, 13–22. <https://doi.org/https://doi.org/10.1016/j.renene.2011.09.002>
- Arunvinthan, S., & Nadaraja Pillai, S. (2019). Aerodynamic characteristics of unsymmetrical aerofoil at various turbulence intensities. *Chinese Journal of Aeronautics*, *32*(11), 2395–2407. <https://doi.org/https://doi.org/10.1016/j.cja.2019.05.014>
- Arunvinthan, S., Nadaraja Pillai, S., & Cao, S. (2020). Aerodynamic characteristics of variously modified leading-edge protuberanced (LEP) wind turbine blades under various turbulent intensities. *Journal of Wind Engineering and Industrial Aerodynamics*, *202*(May 2019), 104188. <https://doi.org/10.1016/j.jweia.2020.104188>
- Arunvinthan, S., Raatan, V. S., Nadaraja Pillai, S., Pasha, A. A., Rahman, M. M., & Juhany, K. A. (2021). Aerodynamic characteristics of shark scale-based vortex generators upon symmetrical airfoil. *Energies*, *14*(7). <https://doi.org/10.3390/en14071808>
- Bodavula, A., Yadav, R., & Guven, U. (2019). Stall mitigation and lift enhancement of NACA 0012 with triangle-shaped surface protrusion at a reynolds number of 10^5 . *SAE International Journal of Aerospace*, *12*(2), 133–151.

- <https://doi.org/https://doi.org/10.4271/01-12-02-0007>
- Das, T. K., & Samad, A. (2020). Influence of stall fences on the performance of Wells turbine. *Energy*, *194*, 116864. <https://doi.org/10.1016/j.energy.2019.116864>
- De Tavernier, D., Ferreira, C., Viré, A., LeBlanc, B., & Bernardy, S. (2021). Controlling dynamic stall using vortex generators on a wind turbine airfoil. *Renewable Energy*, *172*, 1194–1211. <https://doi.org/10.1016/j.renene.2021.03.019>
- Eldredge, J. D., & Jones, A. R. (2019). Leading-edge vortices: Mechanics and modelling. *Annual Review of Fluid Mechanics*, *51*, 75–104. <https://doi.org/10.1146/annurev-fluid-010518-040334>
- Elsayed, A. M., Khalifa, M. A., Benini, E., & Aziz, M. A. (2023). Experimental and numerical investigations of aerodynamic characteristics for wind turbine airfoil using multi-suction jets. *Energy*, *275*, 127503. <https://doi.org/https://doi.org/10.1016/j.energy.2023.127503>
- Güzelbey, İ. H., Eraslan, Y., & Dođru, M. H. (2019). Effects of taper ratio on aircraft wing aerodynamic parameters: a comparative study. *European Mechanical Science*, *3*(1), 18–23. <https://doi.org/10.26701/ems.487516>
- Hao, L., Hu, B., Gao, Y., & Wei, B. (2023). Effect of vortex generator spanwise height distribution pattern on aerodynamic characteristics of a straight wing. *Advances in Aerodynamics*, *5*(1), 1–15. <https://doi.org/10.1186/s42774-023-00137-1>
- Joseph, J., A., Sathyabhama, & Sridhar, S. (2022). Experimental and numerical analysis of humpback whale-inspired tubercles on swept wings. *Aircraft Engineering and Aerospace Technology*, *94*(10), 1577–1592. <https://doi.org/10.1108/AEAT-04-2021-0114>
- Koca, F., & Ozturk, A. (2022). Experimental investigation of the effect of a semi-circular spiral protrusion on the turbulent flow past a cylinder. *Fluid Dynamics*, *57*(3), 371–386. <https://doi.org/10.1134/S0015462822030089>
- Krishnan, S. G., Ishak, M. H., Nasirudin, M. A., & Ismail, F. (2020). Investigation of aerodynamic characteristics of a wing model with RGV winglet. *Journal of Aerospace Technology and Management*, *12*(1), 1–18. <https://doi.org/10.5028/jatm.v12.1108>
- Öztürk, A., Çoban, M., & Koca, F. (2023). Experimental and numerical investigation of the control of the flow structure on surface modified airfoils. *Journal of Applied Fluid Mechanics*, *16*(12), 2381–2395. <https://doi.org/10.47176/jafm.16.12.1996>
- Raj Mohamed, M. A., Yadav, R., & Guven, U. (2021). Flow separation control using a bio-inspired nose for NACA 4 and 6 series airfoils. *Aircraft Engineering and Aerospace Technology*, *93*(2), 251–266. <https://doi.org/10.1108/AEAT-08-2019-0170>
- Rezaeiha, A., Montazeri, H., & Blocken, B. (2019). Active flow control for power enhancement of vertical axis wind turbines: Leading-edge slot suction. *Energy*, *189*, 116131. <https://doi.org/10.1016/j.energy.2019.116131>
- Richard, P. R., John Wilkins, S., & Hall, J. W. (2017). particle image velocimetry investigation of the coherent structures in a leading-edge slat flow. *Journal of Fluids Engineering*, *140*(4). <https://doi.org/10.1115/1.4038091>
- Rossow, V. J. (1992). Two-fence concept for efficient trapping of vortices on airfoils. *Journal of Aircraft*, *29*(5), 847–855. <https://doi.org/10.2514/3.46255>
- Rudenko, S. I., & Ryzhkova, M. V. (1968). Flow on a swept wing in the region of a fence. *Fluid Dynamics*, *3*(6), 84–86. <https://doi.org/10.1007/BF01022888>
- Sundaravadivel, T. A., Nadaraja Pillai, S., & Senthil Kumar, C. (2013a). *Experimental analysis on a wind turbine model with a 3-D span-wise projection for passive flow control*. Proceedings of the 8th Asia-Pacific Conference on Wind Engineering, APCWE. https://doi.org/10.3850/978-981-07-8012-8_277
- Sundaravadivel, T. A., Nadaraja Pillai, S., & Senthil Kumar, C. (2013b). *Influence of boundary layer control on wind turbine blade aerodynamic characteristics – Part I – Computational study*. Proceedings of the 8th Asia-Pacific Conference on Wind Engineering. https://doi.org/10.3850/978-981-07-8012-8_211
- Sundaresan, A., Arunvinthan, S., Pasha, A. A., & Pillai, S. N. (2021). Effect of Ice accretion on the aerodynamic characteristics of wind turbine blades. *Wind and Structures, An International Journal*, *32*(3), 205–217. <https://doi.org/10.12989/was.2021.32.3.205>
- Wang, S., He, G., & Liu, T. (2019). Estimating lift from wake velocity data in flapping flight. *Journal of Fluid Mechanics*, *868*, 501–537. <https://doi.org/10.1017/jfm.2019.181>
- Wang, T., Feng, L. H., & Li, Z. Y. (2021). Effect of leading-edge protuberances on unsteady airfoil performance at low Reynolds number. *Experiments in Fluids*, *62*(10), 1–13. <https://doi.org/10.1007/s00348-021-03310-8>
- Williams, M. D., Reeder, M. F., Maple, R. C., & Solfelt, D. A. (2010). Modeling, Simulation, and Flight Tests for a T-38 Talon with Wing Fences. *Journal of Aircraft*, *47*(2), 423–433. <https://doi.org/10.2514/1.46122>
- Wu, Z., Chen, T., Wang, H., Shi, H., & Li, M. (2022). Investigate the aerodynamic performance of wind turbine blades with vortex generators at the transition area. *Wind Engineering*, *46*(2), 615–629.

<https://doi.org/10.1177/0309524X211038542>

[5249-1](#)

Yang, W. Q., Song, B. F., Song, W. P., & Wang, L. G. (2012). The effects of span-wise and chord-wise flexibility on the aerodynamic performance of micro flapping-wing. *Chinese Science Bulletin*, 57(22), 2887–2897. <https://doi.org/10.1007/s11434-012->

Zhang, K., Hayostek, S., Amitay, M., He, W., Theofilis, V., & Taira, K. (2020). On the formation of three-dimensional separated flows over wings under tip effects. *Journal of Fluid Mechanics*. <https://doi.org/10.1017/jfm.2020.248>